Proceedings of ASME Turbo Expo 2015
GT2015
June 15-19, 2015, Montreal, Canada

GT2015-43192

ACCURATE BLADE TIP TIMING LIMITS THROUGH GEOMETRY MISTUNING MODELING

Alexander A. Kaszynski
Universal Technology Corporation
Dayton, OH 45434
Email: akascap@gmail.com

Jeffrey M. Brown
Turbine Engine Division
U.S. Air Force Research Laboratory
Wright-Patterson AFB, OH 45431

ABSTRACT

Blade tip timing (BTT) is a commonly used non-intrusive stress measurement system to estimate the operational stresses within an engine's rotors without the costly installation of strain gauges that can add additional stiffness to the rotor. BTT systems are now standard on many engine tests and ensure safe operations by avoiding running near maximum rotor stress limits. Since these systems measure blade time of arrival (TOA), processes are applied to first convert this data to displacement and then to stress. This effort focuses on the conversion of displacement to stress where the the classic approach utilizes nominal geometry obtained from an "as-designed" nominal model and creates computes the mode shapes using finite element analysis (FEA). The predicted mode shapes of the cyclic analysis reveal the relationship between maximal blade stress and tip displacement for a given nominally designed rotor. However, manufactured rotors deviate from nominal design due to inherent variability in the machining procedures. It is now possible through high fidelity optical geometry collection systems to obtain more accurate BTT limits using measured IBR geometry from as-manufactured rotors. It will be shown that due to the high variability of blade-to-blade geometry obtained from an optically scanned rotor that the BTT limits can vary significantly between blades. A method is also developed that allows comparisons between cyclic sector and full rotor FEA. This research suggests to optimize BTT probe placement not only to measure the maximum expected deflection given blade tip mode shapes, but also to account to for blade to blade geometric variation.

NOMENCLATURE

BTT	Blade tip timing
CAD	Computer-aided design
CMM	Coordinate measuring machine
DOF	Degrees of freedom
EO	Engine order
FEA	Finite element analysis
FEM	Finite element model
FMM	Fundamental mistuning model
GMM	Geometrically mistuned model
HCF	High cycle fatigue
IBR	Integrally bladed rotor
ND	Nodal diameter
NSMS	Non-intrusive stress measurement system
PCA	Principal component analysis
S/N	Signal to noise ratio
TOA	Time of arrival
$\frac{\sigma_v}{u_c}$	Ratio of maximum vibrational blade stress to measured blade deflection
σ_v	Maximum allowable vibrational von Mises stress

INTRODUCTION

Bladed rotors in turbomachinery are subject to a variety of excitations, both transient and non-transient, during engine operation. These excitations may coincide with the natural frequencies of the rotor's system modes and cause resonances that lead to premature failure from high cycle fatigue (HCF) [1]. Due to the

difficulty in an a priori determination of airfoil vibratory stress, it is necessary to monitor the measured airfoil responses during engine testing. While this can be accomplished using the traditional approach of blade mounted strain gauges, this approach leads to several complications including inaccuracy caused blade stiffening [2], gauge longevity, disruption of airflow, and the high cost and complexity of the additional hardware to interface with the instrumentation. To provide an alternate, simpler, more cost effective real time measurement technique, the turbine engine community has developed a non-intrusive stress measurement system (NSMS) for both engine testing and real time health monitoring commonly known as blade tip timing (BTT) [3].

Blade tip timing conventionally utilizes nominal computer-aided design (CAD) models in combination with finite element analysis (FEA) to obtain mode shape and stress values for rotors operating in either simulated or actual operation. However, as it will be demonstrated, BTT probe limits as well as stress to deflection ratios can vary widely between blades when accounting for actual geometry, especially for higher order modes. This work builds on a variety of research in the area of geometric mistuning [4–6].

This paper proceeds in the following manner: First, the methodology behind conventional BTT will be discussed to provide a basis for the new method developed. Next, conventional BTT limits will be generated for a rotor assuming a nominal, cyclically symmetric integrally bladed rotor (IBR) and will be compared to results from an as-manufactured mistuned rotor finite element model (FEM) generated from optical scan data. After establishing the difference between the two approaches, a straightforward approach will be presented to extract geometrically mistuned sector based BTT limits regardless of the nodal diameter of the mode of interest. The proposed methodology can be applied to any mistuned rotor, integrally bladed or not, to more accurately estimate real-time blade stress using geometrically mistuned models (GMMs).

NON INTRUSIVE STRESS MEASUREMENT - BLADE TIP TIMING

BTT provides real-time TOA data during engine operation using optical or other non-contact probes that compare the actual blade arrival time versus the estimated non-vibrating blade arrival time [7]. This TOA data is then converted to blade tip deflection using straightforward relationships between rotor rotational speed and time. Following this, the tip deflections are related with a maximum vibratory stress using modal analysis results for the modes within the engine's operational range. This process requires an accurate FEM that represents the test rotors to the highest physical and numerical fidelity possible [8].

The standard approach for determining BTT limits requires the computation of the correlation between blade stress and blade tip deflections at the probe measurement points [3]. Rotors in an engine undergo four major loads: centripetal, thermal, steady aerodynamic, and harmonic aerodynamic loading. Each of these loads must be accounted for when determining the maximum acceptable blade tip deflection since HCF is caused by a combination of static and vibratory stress. In a simplified Goodman diagram (Figure 1), the failure region is above the solid diagonal line. The Goodman line for efficiency can be created from the linear interpolation between the ultimate yield strength (x-intercept) and the fully reversed vibrational stress failure point (y-intercept). As an example of the Goodman diagram's use, the stress cloud for a blade of the rotor, shown as the red points in Goodman diagram, indicates the static and vibratory stress state for each node in the FEM for a particular mode. The static stress is constant for a specific operating condition while the vibratory stress is dependent on the deflection of a blade and the mode shape for a given vibratory mode.

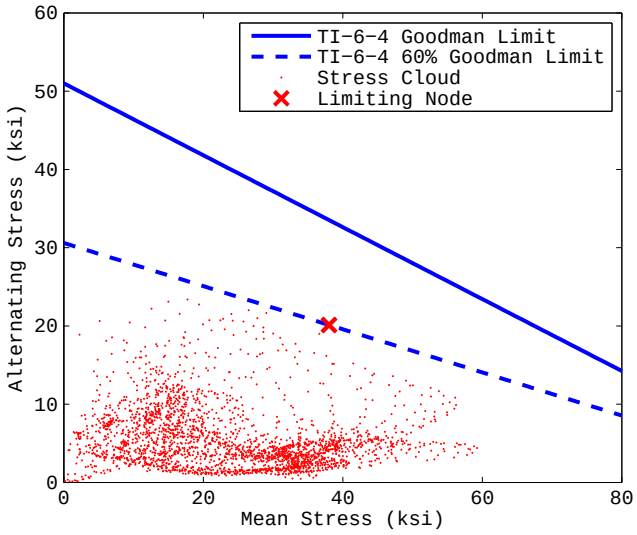

FIGURE 1: Sample Goodman Diagram

Figure 2 shows the BTT test setup for a single blade and single probe of a generic compressor such that the axial direction is vertical on the figure and the circumferential direction is horizontal. The undisturbed blade shown as the dotted airfoil on the right represents the location of the blade with zero vibration energy. The blade offset due to aerodynamic loading and blade untwist due to rotational loading can be accounted for prior to the analysis or otherwise treated as an unknown, though this increases the number of BTT probes required to determine the delta in blade displacement [9]. The location of the undisturbed blade is tracked by a once per revolution or multiple per revolution probe on the rotor shaft, while the deflected position of the blade is determined by comparing the expected TOA to the actual TOA

of the blade via

$$u_c = \omega(t_{\text{actual}} - t_{\text{expected}})r_{\text{tip}} \tag{1}$$

where u_c is the blade circumferential displacement as measured by the probe, ω is the angular velocity of the rotor, t is time, and r_{tip} is the radius at the blade tip at the measurement point. Given the angle of incidence of the blade relative to its circumferential motion, a small perpendicular deflection leads to larger detected displacement of the blade. Therefore, according to the geometry of the blade and the non-transient deflection of the blade, the actual perpendicular blade displacement can only be determined through application of FEA where the solution of the eigenproblem

$$[[K] - \omega^2[M]]X = 0 \tag{2}$$

yields a set of eigenvalues $[\omega_N^2]$ and eigenvectors $[\Psi] = [\psi_1, \psi_2, \cdots \psi_N]$ where N corresponds to the DOF of that system, which for a structural FEM is the DOF per node multiplied by the number of nodes. As each node within the blade sector is undergoing a static stress and as the eigenvector, or mode shape, is unscaled, it is possible to determine the limiting point according

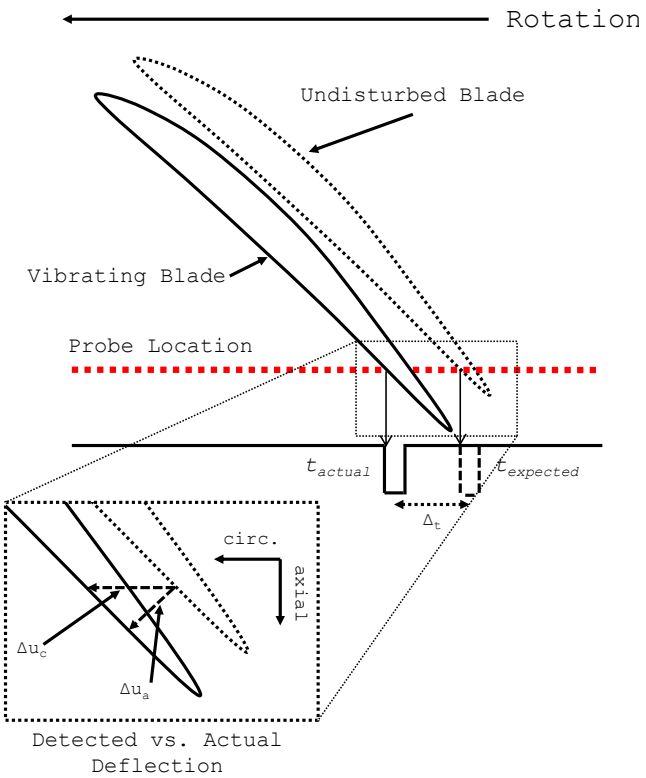

FIGURE 2: BTT Probe and Blade Setup

to the maximal vibrational stress such that

$$\sigma_{v_{\max}}(\sigma_s)\mathrm{f_s} \leq \mathrm{G_e} \tag{3}$$

is made true by scaling the von Mises stress σ_v by factor $\mathrm{f_s}$ such that maximal allowable σ_v as a function of the static stress σ_s falls within the Goodman envelope $\mathrm{G_e}$. Scaling the stress will result in a proportional scaling of the nodal displacement for the mode shape due to the linear relationship between nodal displacement and averaged nodal stress. Using Equation 3 it is possible to determine the shape of the deformed blade given the maximum allowable state of stress within the blade. Conversely, and assuming linear system behavior, a known displacement of any point on the FEM for a given mode shape(eigenvector) for a given mode will allow for the computation of the displacement for all other nodes of the FEM and therefore stress. This is the cornerstone of BTT: that for a particular mode shape knowledge of the displaced position of the blade tip reveals the state of stress for the entire blade.

There are two practical aspects of the FEM to be considered in BTT stress measurement. First, given the discrete nature of a FEM, the intersection point between the BTT probe and the FEM will occur between nodes. Additionally, the spot probe can only detect circumferential displacement of the blade at a specific point axially and independent of the mode shape. To accommodate these factors, the blade displacement for a given mode shape is computed by generating two polynomial fits, one for the loaded static blade, and one for the displaced blade undergoing the same static load. This displacement, u_c, is the detected circumferential displacement. To define BTT limits for each mode, there is an acceptable maximum u_c for a given axial position along the blade.

This paper will deal with a particular type of bladed rotor where the airfoils are integral with the disk as an IBR. Strong coupling between blades of an IBR allow for the formation of strong system modes, and these system modes are excited by synchronous excitations at an integer multiple of the engine's angular velocity. Given the computational time required to solve large DOF problems like a 360° rotor, the traditional approach for modeling an IBR is to assume a cyclically symmetric rotor which assumes that there are no blade to blade variations in geometry or material properties. This allows for the extraction of results at all harmonic indexes for each mode using a model of a single sector. Each harmonic index corresponds to an engine order (EO) excitation from mechanical or aerodynamic effects such as irregular pressure distributions from inlet guide vanes. As this is a known quantity given a particular engine, a Campbell diagram can be constructed for one or many harmonic indexes for all engine operating conditions.

The example Campbell diagram shown in Figure 3 plots the frequency of several rotor system modes for a given harmonic index as well as EO excitations as an integer multiple of the ro-

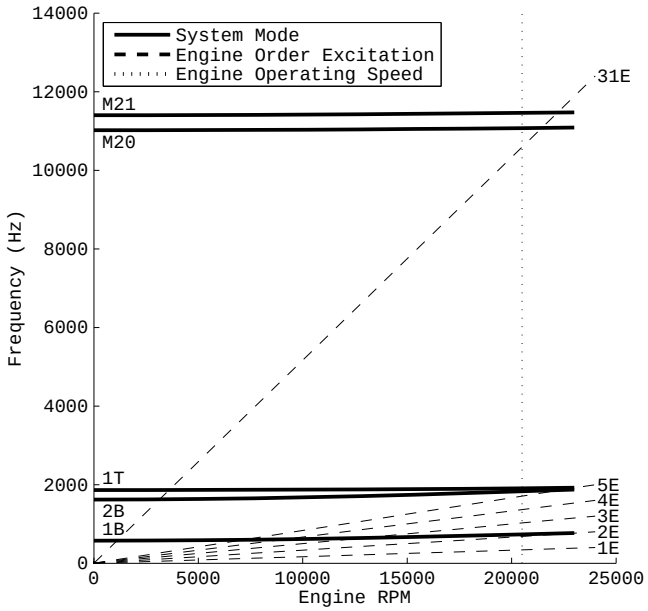

FIGURE 3: Campbell Diagram (Irrelevant Modes Removed)

tor angular velocity. The intersections of the EO excitations and the system modes at the engine operating RPM indicates modes that should be monitored by BTT limits. An engine order excitation pattern will excite a certain nodal diameter (ND) on the IBR and requires a unique Campbell diagram to be generated for that particular ND. This particular figure is representative of the IBR to be introduced in the following section and has 20 blades and upstream hardware that generates engine order excitations at 1 through 5 and 31. The formula to determine the nodal diameter excited given an engine order excitation is

$$\mathrm{ND(EO)} = \begin{cases} \mathrm{EO} & \text{if } \mathrm{EO} \leq \frac{\mathrm{B}}{2} \\ \mathrm{B} - \mathrm{EO} & \text{if } \frac{\mathrm{B}}{2} < \mathrm{EO} \leq \mathrm{B} \end{cases} \tag{4}$$

where B is the number of blades in the rotor and EO is the integer engine order excitation. When EO is greater than B, EO is subtracted by some multiple of B to place EO between 0 and B. For example, EO 31 excites nodal diameter 9 which is the ND of the plot generated in this figure. According to this figure, BTT probe limits would be produced for 1B at 2 ND, 2B and 1T at 5 ND, and M20 and M21 at 9 ND. These probe limits will show the mode shape of the blade when deflected at the maximum allowable stress, and the intersection of the probes and the deflected blade are the maximum allowed deflection limits. BTT limits for 1B at 2 ND can be found in Figure 4, where the actual and measured limits have been computed across the chord of the nominal blade of the IBR and the as measured deflection limits at the probes correspond to the intersections of the dotted black lines and the blue NSMS detected line. During an engine test these probes would be monitored while the rotor is be swept from idle to its normal operating condition to ensure blade stresses remain in an acceptable range.

An ideal cyclically symmetric rotor would respond at only the system modes that resonate at the corresponding EO excitation. However, actual manufactured rotors perform quite differently. Geometric and material variations between blades can lead to a phenomenon known as mistuning, where the modal confinement of energy may lead to HCF and possibly blade failure [10]. Mistuning also breaks down the periodicity of the IBR so that an excitation at a single EO will yield a response at multiple adjacent NDs. These sets of system modes for a given blade mode may overlap one another, requiring the use of additional spot probes to ascertain the mode shape of the blade tip to ascertain the mode shape of the blade tip. Several statistical analysis techniques exist for determining the EO and mode excited during engine testing, to include the determinant method and autoregressive methods [11]. What has not been considered to date is the impact of blade-to-blade geometry variations on the mode shapes used to determine BTT limits. No technique or algorithm exists that accounts for the variation in static and vibrational stress due to mistuning. BTT limits as predicted by a cyclic analysis may, depending on the particularities of a mode shape, be inaccurate due to the as-manufactured rotor variations in blade tip mode shape as well as variations in the static and modal stress. This paper will show that the BTT limits based on the nominal cyclic rotor approach can vary widely from limits generated from geometrically mistuned rotors. This will be demonstrated using a full 360° mistuned rotor FEM as well as isolated mistuned FEMs.

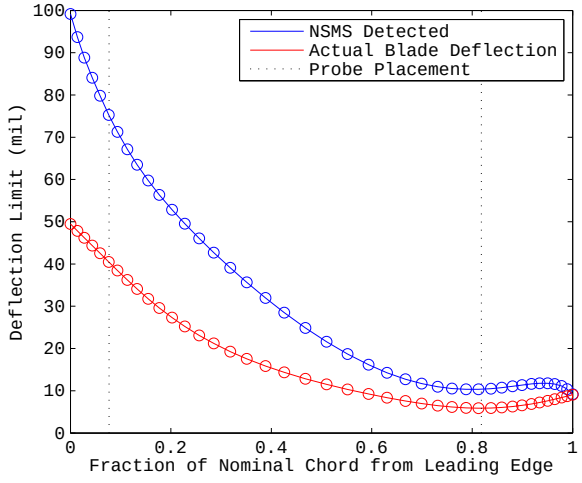

FIGURE 4: Example Blade Tip Deflection Limits

MISTUNED IBR BLADE TIP LIMIT PREDICTION APPROACH

For this paper a single 20 bladed production IBR was chosen for analysis using both the classic tuned and the developed mistuned BTT limit calculation approach. The transonic compressor stage has been researched in the past [12] and the stage composed of 20 low-aspect-ratio rotor blades and 31 stator blades. A representative single sector of the IBR is shown in Figure 5 and contains 95% hexahedral elements and a tetrahedral/pyramidal interface between the blade platform and the remainder of the disk. Quadratic hexahedrals were used to reduce solution time and to increase solution accuracy [13] through the minimization of numerical mistuning [14] when displacing interior and exterior nodes to match the as-manufactured rotor. Cyclic boundary conditions were implemented on the disk sector boundaries as well as a zero-displacement boundary condition on the bore fore and aft faces of both models to match the boundary conditions of the IBR as installed in the engine.

To generate a representative FEM of the as manufactured model, a FEM replica was created through optical topography measurement and mesh morphing. The mesh morphing process begins by generating a full 360° tuned model from a single nominal sector cyclically replicated around the rotor axis. The geometry of this FEM is then morphed to the point cloud geometry collected from the as-manufactured rotor by an optical measurement system.

The optical topography approach was used in this work because it overcomes several disadvantages of legacy coordinate measurement machine (CMM) systems. While CMM are highly accurate, they are limited in their geometry collection rate as well as their collection locations; typically geometry can only be collected from the blade cross sections and not from the blade tips, roots, or the disk interface. Optical scanning systems use structured light and high density charged coupled devices to allow for the rapid acquisition of millions of points of geometry for the entire IBR, creating a "point cloud" where each point represents a surface coordinate on the part of interest. The optical scan of the as-manufactured rotor contained 2×10^6 scan points and an average observable noise of $\pm$ 0.3 mil (25.4 µm) [4].

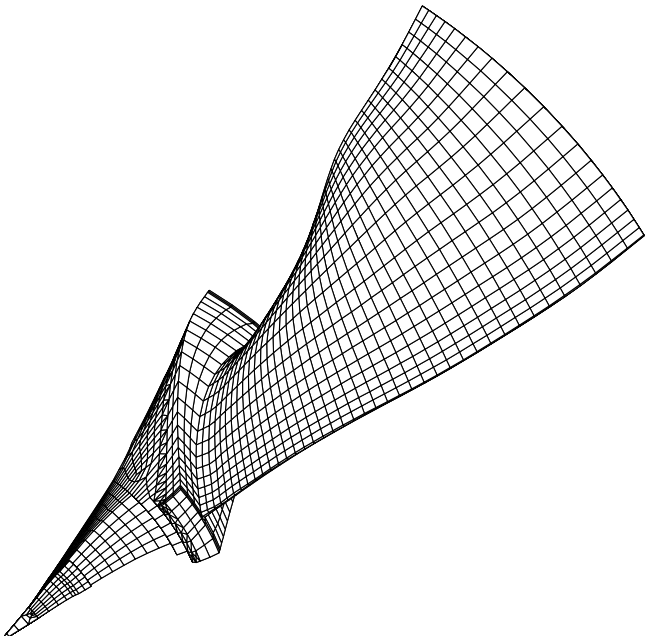

FIGURE 5: Single Sector of the Production IBR FEM

The optical scan data for the rotor was aligned to the existing nominal FEM using an iterative closest point (ICP) procedure. The blades were then geometrically mistuned by modifying the surface nodes to match the tessellated surface data of the point cloud. The specifics of this process can be found in previous research that demonstrated the process on rotors [5]. To summarize, the surface nodes of the FEM are treated as a neural network and iteratively aligned to match the tessellated scanned geometry using local surface curvature and point to surface distances. These global surface displacements are then propagated internally and laterally using a network of radial basis functions thereby preserving element shape and maintaining the integrity of the FEM. This method was verified with similar production rotors through the use of the fundamental mistuning model (FMM) [15, 16] which showed a 0.908 correlation between sector alone frequencies extracted from experimental results and from FEA of the same rotor [6].

Now with two types of models constructed, nominal and GMM, the differences in calculated BTT limits can be determined. Both were applied centripetal loads of 20,000 RPM to account for blade untwist and stiffening due to the pre-stressing of the rotor. Neglecting aerodynamic loads, both pre-stressed models underwent a modal analysis at ND 0 for the first four bending modes.

Unlike the tuned model, the results from the full rotor require further post-processing due to the nature of modal confinement within a mistuned rotor. A system mode exciting a single blade mode for all blades simultaneously, regardless of the simplicity of the system mode, will not result in an equal distribution of energy in a mistuned rotor [17,18]. The natural frequency of the system mode is a combination of the blade alone natural frequencies and the disk. As this natural frequency will not be coincident with each sector's natural frequency, each blade will vibrate at a different intensity. Therefore, the full mistuned rotor modal results will have unequal distribution of vibrational energy throughout its blades.

To account for this, the total vibrational energy in each blade must be computed and the BTT results must be adjusted accordingly. The displacement at similar locations on all blades cannot be used as an accurate measure of energy distribution as blade

TABLE 1: Geometrically Averaged vs. Mistuned BTT Results at ND 0

	Averaged Sector		Full Mistuned IBR	
Mode	$\frac{\sigma_v}{u_c}$ ($\frac{\text{ksi}}{\text{mil}}$)	σ_v (ksi)	$\frac{\sigma_v}{u_c}$ ($\frac{\text{ksi}}{\text{mil}}$)	σ_v (ksi)
1B	0.198	19.90	0.161 - 0.218	17.24 - 21.21
2B	0.239	20.12	0.186 - 0.251	19.43 - 21.08
3B	0.400	25.09	0.341 - 0.458	23.03 - 27.42
4B	0.464	25.92	0.330 - 0.536	24.29 - 27.11

mode shapes vary between mistuned blades and it would be impossible to determine between mode shape or energy distribution as the cause for the variation in blade deflection. Instead, the solution is to compare the relative strain energy in each blade as this is a function of modal energy for a given mode shape. Element strain energy is computed by

$$\mathrm{E}_\varepsilon = \int \frac{1}{2}\varepsilon^\intercal \sigma \mathrm{d}V \tag{5}$$

where the strain energy for a single element E_ε is a function of the strain ε and stress σ within an element integrated over the volume V of the element. As the solution of the eigenproblem yields unscaled eigenvectors describing the mode shape corresponding to the eigenvalue of interest, only the relative values of strain energy need to be compared between blades. To compute Equation 5, the nodal displacements u for all DOF described by eigenvector ψ are related to elemental strain according to

$$\varepsilon_\psi = [\mathrm{B}^\mathrm{e}]\{u_\psi^\mathrm{e}\} \tag{6}$$

where $[\mathrm{B}^\mathrm{e}]$ is the element shape function dependent on the type and geometry of the element and u_ψ^e is a vector of the nodal displacements for that element for that system mode. Assuming a linear solution, elastic stress is related to strain via Hook's Law according to the constitutive matrix $[\mathrm{C}]$ thereby simplifying equation 5. Combining Equations 5 and 6, the strain energy for a blade at a given system mode is the sum of the strain energy in each element according to

$$\mathrm{E}_{\psi\text{blade}} = \sum_{i=1}^{n} \int \frac{1}{2}\left[\mathrm{B}^\mathrm{e}\{u_\psi^\mathrm{e}\}\right]^\intercal [\mathrm{C}]\left[\mathrm{B}^\mathrm{e}\{u_\psi^\mathrm{e}\}\right]\mathrm{d}V \tag{7}$$

where blade strain energy is a function of only the mode shape ψ and the element shape functions B^e.

Using this approach for the full mistuned model the maximum blade stress and maximum blade stress to deflection were calculated for probes placed at 11% and 92% of the cold axial chord and the results for the first probe can be found in Table 1. The maximum allowable von Mises vibrational stress for the blade is listed as σ_v in ksi, and the ratio between the measured deflection at the probe and the maximum blade stress is listed as $\frac{\sigma_v}{u_c}$ in ksi per mil. Results in SI units can be found in the Appendix. The results from the mistuned IBR show significant variation from the tuned rotor even for these lower energy bending modes. For example, the maximum allowable blade stress varied from 24.29 to 27.11 ksi for 4B and the deflection to stress ratio varied significantly between 0.330 and 0.536 ksi per mil, which is -28.84% to 15.66% from the tuned results. These deflection to stress variations are caused by not only variations in the mode shape of the blade but also in the stress distribution throughout the blade.

Variations in blade to blade geometry due to mistuning lead to variations in both the magnitude and location of vibrational and static stress thereby changing the shape of the "stress cloud" as shown in example Figure 1 in a non-trivial manner. Furthermore, the variation in mode shape changes the deflection of the blade tip as seen by the BTT probe, especially for the higher order modes. For example, Figure 6 shows there is considerable variation between the tuned and the mistuned blade deflection limit results for a high order mode. This figure shows six out of 20 mistuned blade results for clarity. Accounting for variations in mode shape could significantly increase the accuracy of the data reduction from the BTT probe results. This could be accomplished not only by placing the probes in a location which more fully captures the variable mode shapes of a mistuned rotor, but also in the post processing phase as the variation in mode shape can greatly effect results obtained by an extraction method such as Prony's method or Multiple Revolution Formulation [9].

Furthermore, it may not even be necessary to reverse engineer a rotor in order to evaluate the sensitivity of geometric

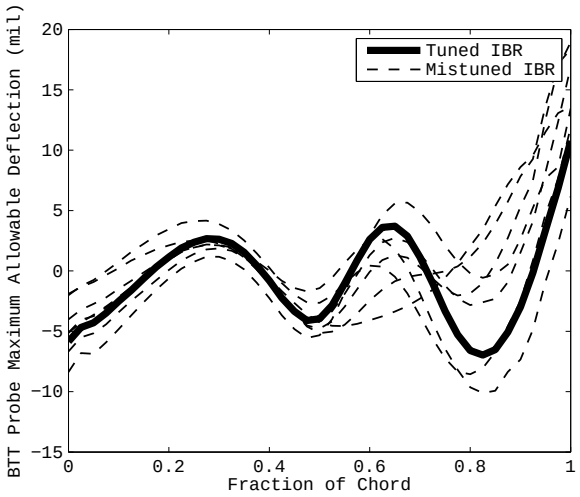

FIGURE 6: BTT Probe Limits for a High Order Mode

variations on BTT limits; a geometry based Monte Carlo simulation could allow for an estimation of mode shape variations for higher order modes, though a principle component analysis (PCA) based on a population of scanned rotors would provide a more accurate estimate in the variation of BTT limits as it would reflect actual geometric variations between blades.

The results thus far have been limited to ND 0 in which all blades are vibrating in-phase. This is because the modal analysis from all other NDs from a full mistuned IBR cannot be utilized due to modal confinement. In a perfectly tuned rotor the natural frequencies for all but ND 0 and ND $\frac{N}{2}$ exist in pairs in which the mode shapes for each pair are exactly 90° out of phase. The square root of the sum of the displacements and stresses of the pairs reveals the state of displacement and stress for that mode at that nodal diameter. While such pairs exist for a mistuned rotor, blade to blade mistuning allows for one or many blades to become a tuned absorber for that mode, resulting in the confinement of vibrational energy in a limited portion of the rotor. This makes the identification and blade alone mode shape recovery of all but the most trivial nodal diameters impossible.

This is significant problem considering that most excitations will not at EO 0. One solution is to isolate and analyze each individual mistuned blade in a pre-stressed cyclically symmetric modal analysis. This effectively analyses each individual blade as a tuned IBR with that isolated blade's geometry and allows for the extraction of higher order NDs while accounting for geometric variance. However, it must be determined if blade to blade interactions within a full IBR vary the mode shapes of its individual blades versus a single isolated blade sector of that model treated as a cyclic model. To make this comparison the vibrational and static stress was outputted for 1B at ND 0 from a single blade from the full IBR modal analysis and compared to the results from that same blade when isolated in a cyclic modal analysis. The stress clouds from both analyses can found in Figure 7, and despite that both results have been scaled independently to keep vibrational stress within Goodman limits, the results are nearly identical with a 0.0254% variation in static stress and a 0.0495% variation in vibrational stress. Mode 1B at ND 0 was used for the comparison as it has the smallest variation in modal energy distribution due to high disk participation and a much smaller relative strength of the system mode versus the blade mode, thereby interfering with isolated blade motion and minimizing modal confinement. These results indicate that blade mode shape is unaffected by blade/rotor integration.

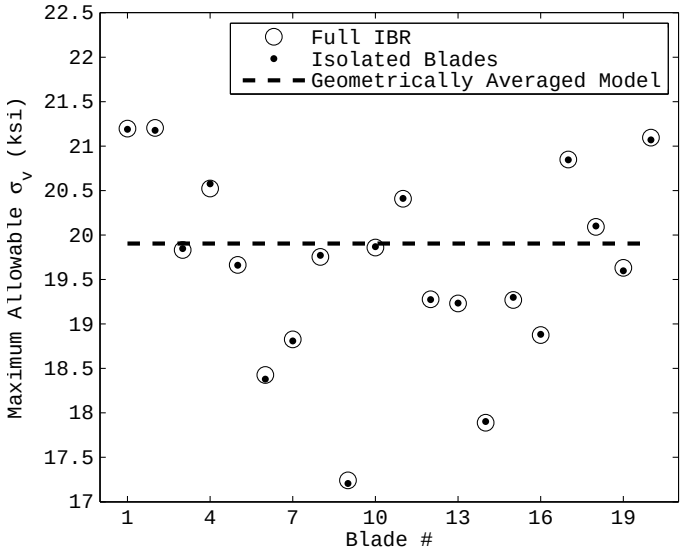

FIGURE 8: Comparing the Maximum Allowable Stress for 1B

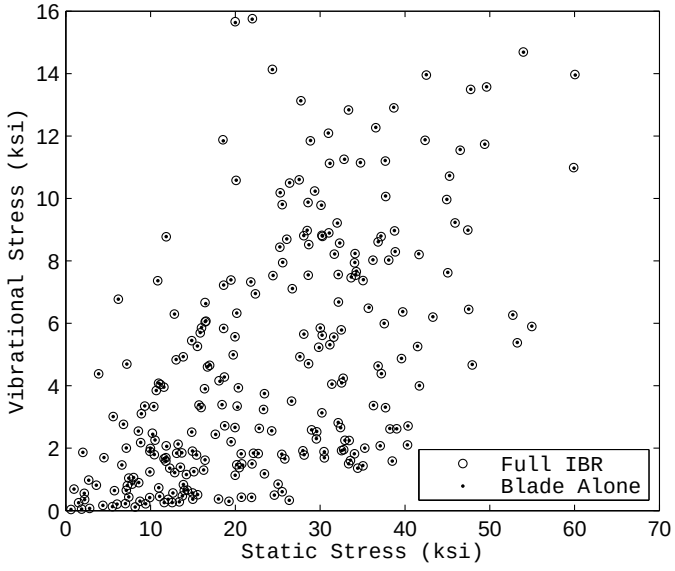

FIGURE 7: State of Stress in Single Isolated and Full IBR Blade

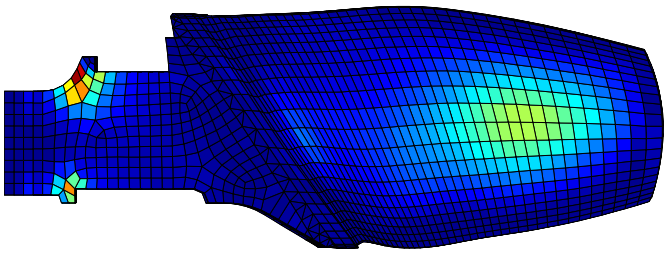

FIGURE 9: Variation in Strain Energy for Blade Sector

TABLE 2: BTT Results for Averaged, Full Mistuned, and Isolated Mistuned Models

		Averaged Sector		Full Mistuned IBR		Isolated Mistuned Sectors	
Mode	ND	$\frac{\sigma_v}{u_c}$ $(\frac{\text{ksi}}{\text{mil}})$	σ_v(ksi)	$\frac{\sigma_v}{u_c}$ $(\frac{\text{ksi}}{\text{mil}})$	σ_v(ksi)	$\frac{\sigma_v}{u_c}$ $(\frac{\text{ksi}}{\text{mil}})$	σ_v(ksi)
1B	0	0.198	19.90	0.161 - 0.218	17.24 - 21.21	0.161 - 0.218	17.21 - 21.19
1B	2	0.189	19.83			0.152 - 0.210	17.69 - 21.27
2B	0	0.239	20.12	0.186 - 0.251	19.43 - 21.08	0.186 - 0.251	19.42 - 21.09
2B	5	0.293	17.95			0.269 - 0.342	16.25 - 18.72
1T	5	0.592	20.12			0.454 - 0.655	19.42 - 21.81
3B	0	0.400	25.09	0.341 - 0.458	23.03 - 27.42	0.359 - 0.461	23.08 - 27.30
4B	0	0.464	25.92	0.330 - 0.536	24.29 - 27.11	0.336 - 0.536	24.26 - 27.11
M20	9	6.384	26.95			3.218 - 47.57	25.28 - 28.24
M21	9	25.748	28.28			8.317 - 67.34	26.72 - 29.39

Having established the invariance of mode shapes between a full rotor and a blade from an isolated blade sector, BTT limits were computed for each one of the 20 isolated blade sectors. This was accomplished by using the same approach and assumptions as in the tuned IBR except with modified geometry. The results for 1B at ND 0, found in Figure 8, show that there is a 99.98% correlation between the full mistuned rotor and the isolated blade sectors for maximum allowable blade stress. The other three bending modes show a 99.07%, 99.31%, and 99.62% correlation in the maximum allowable blade stresses for 2B through 4B. The small variation between these results can be explained by comparing the normalized element strain energy between the isolated and full models for a single blade sector. Figure 9 shows the variation in strain energy between a sector from a full IBR and that same sector in an isolated cyclic analysis for 2B at ND 0 after normalizing the full model for strain energy variation. This figure indicates that the distribution of strain energy within a full model varies not only between blades but within a blade itself, at least compared to its isolated counterpart (and at a maximum of 0.16% for this mode). Therefore, despite accounting for strain energy variance between blades, the results from a full mistuned IBR will include modal energy confinement within an individual sector. As the mode shapes of the isolated and integrated blade are nearly identical, this can be the only remaining reason for the variation between the BTT results. Therefore, it is the confinement of vibrational energy and not a variation between the FEMs that generates dissimilar results between the full and isolated results.

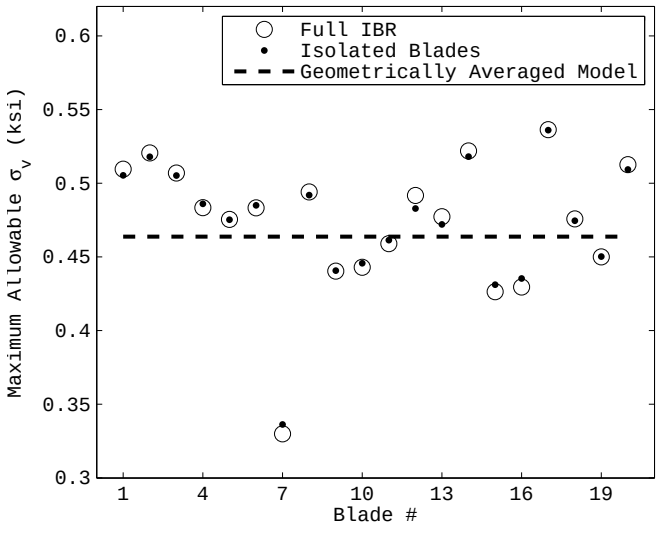

FIGURE 10: Deflection to Maximal Stress for 4B at ND 0

Despite these variances, the models strongly correlate (99.8%) in deflection to stress ratios as shown in Figure 10 for the 4$^{\text{th}}$ bending mode. This is despite the fact that the blade deflection to maximal blade stress ratio is more sensitive to mistuning as both the maximum stress and the mode shape of the blade tip vary. Given the strong correlation of these results it can be assumed that a set of isolated mistuned blades can be substituted for a full mistuned rotor, enabling mistuned BTT limits to be generated for more complex modes at higher nodal diameters from a mistuned IBR.

UTILIZING BTT RESULTS FROM A MISTUNED IBR

The previous section established that individual sectors from a full mistuned IBR can be isolated and analyzed without corrupting blade mode shapes relative to a full IBR analysis. This is a crucial discovery as limits generated from the traditional BTT

approach rely solely on the mode shapes generated from a cyclically symmetric pre-stressed modal analysis. While a modal analysis of a full 360° IBR can indicate the degree of modal confinement and likelihood of mistuning amplification, the invariance of sector-evaluated mode shapes allows for the accurate computation of BTT limits for a mistuned IBR at non-zero nodal diameters and for complex mode shapes. As the purpose of establishing BTT ratios is to accurately measure the maximum allowable blade vibrational stress and its relationship to blade tip deflection, it is the accurate computation of the blade mode shapes and stress cloud that matters. Therefore, it is the determination of the ratio of blade tip deflection to the state of vibrational stress within all blades that must accurately bounded in the case of a mistuned rotor.

The analysis of the IBR in the previous section was expanded beyond low order symmetric system modes to the modes of interest previously identified in the Campbell diagram from Figure 3. The results in Table 2 indicate that the variations in both the maximum blade vibrational stress σ_v and the deflection to maximum vibratory stress ratio $\frac{\sigma_v}{u_c}$ increased for both the higher order modes and for the higher nodal diameter modes. The lower order modes showed larger variations in the σ_v while the higher order modes showed significant variations in $\frac{\sigma_v}{u_c}$. In fact, while the σ_v for mode 21 varied marginally between -5.52% and 3.93% from the tuned rotor, $\frac{\sigma_v}{u_c}$ varied significantly between -67.70% and 161.53% from the tuned results. This large variance in allowable displacements and $\frac{\sigma_v}{u_c}$ could create false positives and negatives during engine testing when assuming a nominal 25.75 ksi per mil deflection based on "as-designed" geometry. It is common during engine testing to place an additional factor of safety on the BTT limits in addition to the 60% reduction in the Goodman limits, and this indicates BTT limits are either overly conservative, or more likely, understood to be rough estimations given unknown blade geometry and mode shape variability. However, given better BTT probe placements and more accurate modeling of blade mode shapes it may be possible to reduce the factor of safety in BTT limits and better ascertain EO excitations taking place within an engine test.

Part of the variation in the deflection to stress ratio is due to the interplay between static stress and vibrational stress which changes the maximum allowable vibrational stress in the blade, and this is the main reason for the variability in displacement to stress ratio in low order modes. High order modes, however, are mostly influenced by the variation in the blade tip mode shape. This is illustrated by Figures 11 and 12, where the lower energy mode exhibits low variations in allowable blade tip deflection and mode shape while mode 21 at ND 9 shows high variability. Probes placed at their original positions at 11% and 92% will result in inaccurate results for this high energy mode despite having been sufficiently accurate for the original tuned model.

Deflection measured by BTT spot probes are also used to indicate both the mode and EO excited at various engine velocities. Clearly, the existing probes at 11% and 92% will be unable to accurately measure the mode shape of the rotor given the large variation of blade mode shapes at those positions for the higher order mode. The results from the mistuned isolated sectors can be used to establish more optimal probe positioning in order to more accurately recover actual EO excitations during

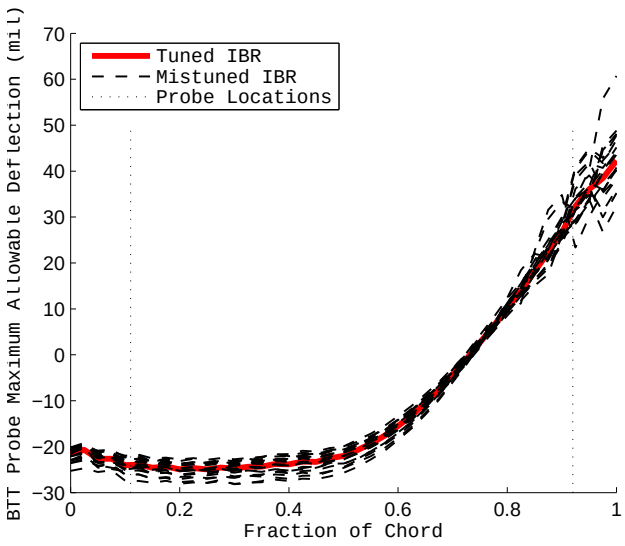

FIGURE 11: Variation in BTT Maximal Deflection and Mode Shape at Blade Tip for 3B at ND 0

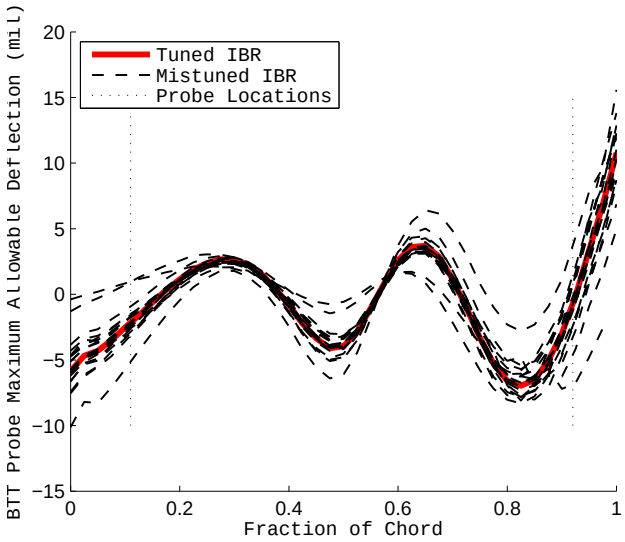

FIGURE 12: Variation in BTT Maximal Deflection and Mode Shape at Blade Tip for Mode 21 at ND 9

TABLE 3: Reduction In Mode Shape Variance with Intelligent Probe Placement

		Probe A Maximum u_c				Probe B Maximum u_c			
		11%		30%		92%		81%	
Mode	ND	μ (mil)	σ (mil)	μ (mil)	σ (mil)	μ (mil)	σ (mil)	μ (mil)	σ (mil)
1B	2	104.119	4.965	100.090	2.725	52.851	1.344	62.946	1.360
2B	5	60.623	3.466	61.095	2.043	26.313	2.297	34.296	2.133
1T	5	34.242	3.929	9.748	1.822	13.938	1.071	11.878	1.255
M20	9	4.014	2.171	4.196	0.821	1.055	0.163	2.939	0.530
M21	9	1.382	0.782	3.005	1.100	0.669	0.779	1.300	0.545

engine testing. The number and location of BTT probes depends on the number and shape of modes observed during an engine test. Highly variable results such as those presented in Figure 12 indicate that more than two probes may be necessary, but as additional hardware increases the cost and complexity of an engine test, it would be best to limit the number of probes to the minimum necessary to correlate blade mode shape and ensure safe engine operation. As such, one approach to limit the number of BTT probes required for testing would be to analyze the signal to noise ratio of the mistuned blade tip mode shapes to determine optimal probe positioning across a series of modes.

The maximization of the measurement signal to noise (S/N) ratio is critical to accurate NSMS. While most approaches seek to maximize S/N at the measurement stage [19], this research indicates that blade tip mode shape variability might produce deflections that would appear noisy to even the most accurate sensors for higher order modes. One approach to improve the accuracy of measured would be to minimize measurement error as well as measured mode shape error by placing probes at locations where the blade mode shape would be the least invariant across all blades and at the points of highest possible deflection. Figure 13 shows the results of Figure 12 but plotted with an additional line indicating the ratio between the maximum blade deflection and the variance in mode shape across all blades. To improve this plot the mean blade deflection limits its $\pm 1\sigma$ have been shown instead of the simultaneous plot of all 22 blades. From this figure it is apparent that the BTT spot probes would be more optimally placed at 30% and 81% cold chord for mode 21. This would enable the accurate detection of this mode while identifying the correct engine order excitation since the blade measured response would be less dependent on blade mistuning. As high order engine modes, especially closely spaced modes such as modes 20 and 21, are the most difficult modes to identify due to small blade deflections, better probe positioning based on mistuned rotor results can help enable accurate mode identification despite inherent rotor mistuning.

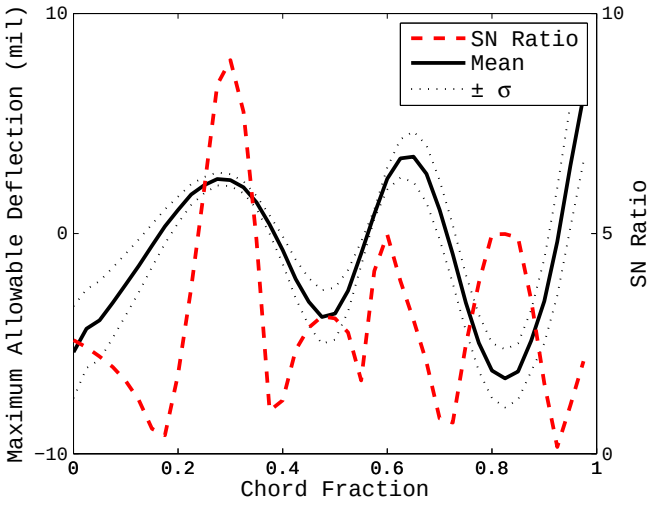

FIGURE 13: Optimal Sampling Locations for Mode 21

Repositioning the BTT probes using the isolated mistuned blade analysis resulted in an improvement in the ratio between maximum allowable blade deflection u_c and the standard deviation among the allowable blade deflections σ. The results shown in Table 3a show the drop in the variance of the results and an increase in the mean maximum deflection by accounting for blade mode shape variance within a mistuned IBR. As the maximum allowable deflections for the higher order modes are strongly correlated with the blade tip mode shape, their maximization will reduce the effective mode measurement noise and make the nodal diameter response of the rotor more apparent during post-processing.

CONCLUSION

This paper has demonstrated that BTT limits obtained from the standard tuned rotor approach can vary widely from the ra-

tio of maximal blade stress to blade tip deflection for a mistuned rotor. It has been demonstrated that it is possible to analyze a mistuned IBR on a sector by sector basis in order to extract blade mode shapes for higher order modes that are impossible to extract using a full model. To the author's knowledge, this is the first demonstration of a methodology to extract BTT limits for a geometrically mistuned rotor. Further research should include an approach to estimate BTT post processing error in extracting engine orders exhibited in recorded BTT sensor results as well as optimization in improving BTT allowable limits. Given a better understanding of the variation between blade mode shape and allowable vibrational stress, the BTT factor of safety margin could be reduced using a mistuned IBR analysis. The next step to this research will be to validate the presented results with experimental engine results to demonstrate blade mode shape variability and more accurate mode shape identification using a probe placement approach that accounts for blade mistuning.

While this research utilized actual part geometry, several other approaches exist to generate mistuned rotor results, to include utilizing a Monte Carlo simulation on blade surface geometry. If attempting to model a large rotor population, it may also be possible to use PCA to extract dominant modes from a limited set of optical (or CMM) reverse engineered geometry and then bootstrap those modes to simulate a theoretical population. This would enable more accurate real-time NSMS on operational platforms to more accurately measure blade tip mode shapes and maximal blade stresses by predicting potential future IBR geometry and its effects on the NSMS measurements.

REFERENCES

[1] Heath, S., Slater, T., Mansfield, L., and Loftus, P., 1997. "Turbomachinery blade tip measurement techniques". In Proceedings 598 on Advanced Non-Intrusive Instrumentation for Propulstion Engines.

[2] Klauke, T., Kuhhorn, A., Beirow, B., and Parchem, R., 2008. "Blade vibration phenomena of hpc bliscs considering manufacturing effects and strain gauge application". In ASME Turbo Expo 2008: Power for Land, Sea, and Air.

[3] Szczepanik, R., Przysowa, R., Spychala, J., Rokicki, E., Kazmierczak, K., and Majewski, P., 2012. *Thermal Power Plants: Application of Blade-Tip Sensors to Blade-Vibration Monitoring in Gas Turbines*. Intech.

[4] Kaszynski, A., Beck, J., and Brown, J., 2013. "Uncertainties of an automated optical 3d geometry measurement, modeling, and analysis process for mistuned integrally bladed rotor reverse engineering". *Journal of Engineering for Gas Turbines and Power,* ***135***.

[5] Kaszynski, A., Beck, J., and Brown, J., 2014. "Automated finite element model mesh updating scheme applicable to mistuning analysis". In ASME Turbo Expo.

[6] Kaszynski, A., Beck, J., and Brown, J., 2015. "Validation and improvement of morph - an automated mistuned finite element updating scheme". In ASME Turbo Expo.

[7] Salhi, B., Lardis, J., Berthillier, M., Voinis, P., and Bodel, C., 2008. "Modal parameter identification of mistuned bladed disks using tip timing data". *Journal of Sound and Vibration,* ***314***(35), pp. 885 – 906.

[8] Liu, C., and Jiang, D., 2012. "Improved blade tip timing in blade vibration monitoring with torsional vibration of the rotor". *Journal of Physics: Conference Series,* ***364***(1), p. 012136.

[9] Gallego-Garrido, J., Dimitriadis, G., and Wright, J. R., 2007. "A class of methods for the analysis of blade tip timing data from bladed assemblies undergoing simultaneous resonances-part i: Theoretical development". *International Journal of Rotating Machinery*.

[10] Castanier, M., and Pierre, C., 2006. "Modeling and analysis of mistuned bladed disk vibration: Current status and emergin directions". *Journal of Propulsion and Power,* ***22***(2).

[11] Gallego-Garrido, J., Dimitriadis, G., and Wright, J. R., 2007. "A class of methods for the analysis of blade tip timing data from bladed assemblies undergoing simultaneous resonances-part ii: Experimental validation". *International Journal of Rotating Machinery*.

[12] Hah, C., Puterbaugh, S. L., and Copenhaver, W. W., 1997. "Unsteady aerodynamic flow phenomena in a transonic compressor stage". *Journal of Propulsion and Power,* ***13***(3), pp. 329 – 333.

[13] Benzley, S. E., Perry, E., Merkley, K., Clark, B., and Sjaardema, G., 1995. "A comparison of all hexagonal and all tetrahedral finite element meshes for elastic and elasto-plastic analysis". In Proceedings, 4th International Meshing Roundtable, pp. 179–191.

[14] Beck, J., Brown, J., Slater, J., and Cross, C., 2012. "Probabilistic mistuning assessment using nominal and geometry based mistuning methods". *Journal of Turbomachinery,* ***135***(5), October.

[15] Feiner, D., and Griffin, J., 2004. "Mistuning identification of bladed disks using a fundamental mistuning model-part 1: Theory". *Journal of Turbomachinery,* ***126***(1), March, pp. 150–158.

[16] Feiner, D., and Griffin, J., 2004. "Mistuning identification of bladed disks using a fundamental mistuning model-part 2: Application". *Journal of Turbomachinery,* ***126***(1), March, pp. 159–165.

[17] Brown, J., and Beachkofski, B., 2000. "A phenomenological investigation of sequence effects on mistuned rotor response". In AIAA/ASME/SAE/ASEE Joint Propulsion Conference.

[18] O'Hara, R., and Brown, J., 2004. "Experimental investigation of geometric uncertainty effects on blade forced response". In AIAA/ASME/SAE/ASEE Joint Propulsion Conference.

[19] Lawson, C. P., and Ivey, P. C., 2005. “Tubomachinery blade vibration amplitude measurement through tip timing with capacitance tip clearance probes”. *Sensors and Actuators A: Physical,* ***118***(1), pp. 14 – 24.

Appendix A: Tables in SI Units

TABLE 1A: Geometrically Averaged vs. Mistuned BTT Results at ND 0 in SI

	Averaged Sector		Full Mistuned IBR	
Mode	$\frac{\sigma_v}{u_c}$ $(\frac{\text{MPa}}{\text{mm}})$	σ_v (MPa)	$\frac{\sigma_v}{u_c}$ $(\frac{\text{MPa}}{\text{mm}})$	σ_v (MPa)
1B	53.75	137.2	43.70 - 59.18	118.9 - 146.2
2B	64.88	138.7	50.49 - 68.13	134.0 - 145.3
3B	108.6	173.0	92.56 - 124.3	158.8 - 189.1
4B	126.0	178.7	89.58 - 145.5	167.5 - 186.9

TABLE 2A: BTT Results for Averaged, Full Mistuned, and Isolated Mistuned Models in SI Units

		Averaged Sector		Full Mistuned IBR		Isolated Mistuned Sectors	
Mode	ND	$\frac{\sigma_v}{u_c}$ $(\frac{\text{MPa}}{\text{mm}})$	σ_v(MPa)	$\frac{\sigma_v}{u_c}$ $(\frac{\text{MPa}}{\text{mm}})$	σ_v(MPa)	$\frac{\sigma_v}{u_c}$ $(\frac{\text{MPa}}{\text{mm}})$	σ_v(MPa)
1B	0	53.74	137.2	43.70 - 59.17	118.8 - 146.2	43.70 - 59.17	118.6 - 146.0
1B	2	51.30	136.7			41.25 - 57.00	121.9 - 146.6
2B	0	64.87	138.7	50.48 - 68.13	133.9 - 145.3	50.48 - 68.13	133.8 - 145.4
2B	5	79.53	123.7			73.01 - 92.83	112.0 - 129.0
1T	5	160.6	138.7			123.2 - 177.7	133.8 - 150.3
3B	0	108.5	172.9	92.56 - 124.3	158.7 - 189.0	97.44 - 125.1	159.1 - 188.2
4B	0	125.9	178.7	89.57 - 145.4	167.4 - 186.9	91.20 - 145.4	167.2 - 186.9
M20	9	1732	185.8			873.5 - 12912	174.2 - 194.7
M21	9	6989	194.9			2257. - 18279	184.2 - 202.6

TABLE 3A: Reduction In Mode Shape Variance with Intelligent Probe Placement in SI Units

		Probe A Maximum u_c				Probe B Maximum u_c			
		11%		30%		92%		81%	
Mode	ND	μ (mm)	σ (mm)	μ (mm)	σ (mm)	μ (mm)	σ (mm)	μ (mm)	σ (mm)
1B	2	2.645	0.126	2.542	0.069	1.342	0.034	1.599	0.035
2B	5	1.540	0.088	1.552	0.052	0.668	0.058	0.871	0.054
1T	5	0.870	0.100	0.248	0.046	0.354	0.027	0.302	0.032
M20	9	0.102	0.055	0.107	0.021	0.027	0.004	0.075	0.013
M21	9	0.035	0.020	0.076	0.028	0.017	0.020	0.033	0.014